Other Research

Development on Quasi-precipitation model for Assessing the River Impact of Global Warming

Contact Person: Masakazu Fujikane
Hydrology Division, River Department of Public Works Research Institute, Ministry of Construction of Japan

Key Words: Global Scale Climate Change (Global Warming), Stochastic method, Quasi-Precipitation, Synoptic Climatology, River Discharge

1. Background

It is predicted that increasing of green house gas such as carbon dioxide cause global climate change. It is usually called global warming. However climate change is not only warming. It is possible to change hydrological cycles in river cathment scale for example precipitation amount, rainfall pattern, evapo-transpiration, soil moisture, water use, etc. Therefore we, water side engineers, have to consider with its impact to make future river plans (design flood, water resource management etc.).

It takes long time (approximately 15 to 30 years) to accomplish building the river facility such as river bank, gate, dam. However the IPCC Scientific Assessment says that concentration of green house gas will become 2 times in 2010s under business as usual scenario (in 2050s under Scenario D). Therefore we have to estimate climate change impact to river cathment area immediately.

However climate change predictions have much uncertainty. General Circulation Models (GCMs) are known to be most reliable method to predict the global climate change, but we can not estimate the cathment scale change using even GCM because of spatial accuracy of the model.

2. Objective

Our objectives of this study are: to develop stochastic model that generates quasi-precipitation in regional scale, and to take seasonal effect into this model in order to calculate the river discharge using runoff model.

This model uses 2 type of precipitation data. One is precipitation output of GCM and other is observed time series of precipitation data at the station in specific cathment because we can estimate the spatial and periodic average change of precipitation due to climate change from GCM output. We can also grasp the regional characteristics of precipitation in cathment from observed data. Stochastic method combines these two types of information.

Further we have to consider the seasonal pattern of Japanese precipitation such as rainy season (Baiu), typhoon and snow in order to calculate the river discharge under global warming condition. Because we have to calculate the river discharge from precipitation data using runoff model whose parameters are determined using observed precipitation and discharge data. Observed precipitation data is reflected the Japanese weather pattern.

3. Methods

3.1 Concept of Stochastic Quasi Precipitation Generating Model

Stochastic quasi precipitation generating model is refereed to Storm Based Model (Beven, 1992). Distribution of consecutive no precipitation day, consecutive precipitation day and total amount during consecutive precipitation day are considered to fit the exponential distribution. Distribution of daily precipitation during consecutive precipitation day is considered to fit the normal distribution. Equations are shown as follows;

$g = 1 - ln(n) * (g_{ave} - 1)$ ... (1)

$d = 1 - ln(n) * (d_{ave} - 1)$ ... (2)

$i = 1 - ln(n) * (i_{ave} - 1)$ ... (3)

$p_n = i + e_n$ ... (4), if $|e_n|$ is grater than $0.9 * i$ then $e_n = (e_n / |e_n|) * 0.9 * i$ ... (5)

where *g: consecutive* no rain day, *gave: average* of consecutive no rain day, *d: consecutive* rain day, *dave: average* of consecutive rain day, i: rainfall intensity during consecutive rain day(mm), i_{ave}: average of rainfall intensity during consecutive rain day, *pn:* daily based rainfall time series during consecutive rain day. *n: uniform* random variables, *en: standard* normal random variables, initial condition assume no rain.

3.2 Area and Data of Study

Area of study is URATSUKUBA experimental Basin (Yamaguchi River, Catchment area = 3.12km^2). Daily based precipitation data of SOFUGAMINE station is used as observed precipitation data (1969 to 1991, 8400 days) and 3 years (1095 days) outputs of Meteorological Research Institute Atmospheric General Circulation Model (hereinafter MRI-GCM) is used as GCM data. In this study, we use only one grid data of 140°E, 38°N from MRI-GCM. Boundary conditions of Calculation at global warming in MRI-GCM are 2 times of CO_2 concentration and 2°C increasing of average sea surface temperature.

3.3 Generation method on precipitation at global warming

Values of g_{ave}^O, $dave^O$, $iave^O$ (o means observation) are calculated from URATSUKUBA data and execute monte-carlo simulation in 100 times to reproduce the 8400 day's precipitation. In next, g_{ave}^1, $dave^1$, $iave^1$ is calculate from output of present condition and g_{ave}^2, $dave^2$, $iave^2$ is calculate from output under warming condition from MRI-GCM (1 means $1*CO_2$ and 2 means $2*CO_2$). Further we calculate g_{ave}^W, $dave^W$, $iave^W$ by equation (6) and execute monte-carlo simulation in 100 times to product the 8400 day's precipitation under warming condition.

$X_{avg}^W = (X_{avg}^2 / X_{avg}^1) * X_{avg}^O$ ... (6) (*X means g, d and i*)

Therefore we can get simulated output on R1 and R2. R1 means simulated precipitation under $1*CO_2$ and R2 is under $2*CO_2$. Number of outputs is 840,000 respectively (8400 days * 100 time's simulation).

4. Result

Table 1 and 2 shows both characteristics of precipitation about URATSUKUBA and MRI-GCM. In Table 2, we are able to estimate that period of drought will be long.

Table 1 Average Precipitation

URATSUKUBA	1454.5 mm
GCM(1*CO2)	1915.5 mm
GCM(2*CO2)	2110.0 mm

Table 2 Model Parameter

	gave	dave	iave
URATSUKUBA	4.21	2.21	11.15
GCM(1*CO2)	2.02	4.85	7.28
GCM(2*CO2)	2.16	4.68	9.84
URATSUKUBA under Global Warming	4.50	2.13	15.07

Concentration and intensity of daily precipitation will be higher under global warming condition. Table 3 shows *average result of monte-carlo simulation. Further we sort* the R1 and R2 in order of increasing. So we can get the 100 data of each order (1 to 8400). We call the data R'1(i, j) and R'2(i, j) (i means number of order, 1 to 8400 and j means simulation number, 1 to 100). We can describe the increasing of high intensity of rainfall under global warming condition as these results of this model.

Table 3 Annual average of simulation (mm)

R1	1560.8
R2	2141.6

5. Adding the Seasonal Effect to Stochastic Model

5. 1 Creating Transition Matrix of Weather Pattern in each month in Japan

Classification method using weather pattern is used pressure pattern classification method (M. Yoshino, 1969). In this study, number of classification is 15 (See Table 4). Collecting the classified calendar from 1961 to 1985, we create the transition matrix of weather pattern in each month in Japan by assuming markov chain about transition of each day's weather pattern (this matrix is 15*15, shows transition i to j of weather pattern as row i to column j).

Table 4 Weather pattern classification

I	**high-east-low pattern**	1
II	**Troug h** Low is passing over Hokkaido or Sakhalin	2
	Low is passing in NE direction over sea of Japan-	3
	Low is passing from Taiwan in E - ENE direction along the Pacific coasts of Japan, under the condition of very deep trough over Japan	4
	Low are passing simultaneously along Japan Sea and the Pacific coasts of Japan, under condition of very deep through over Japan	5
III	**Migratory anticyclone pattern** Passing over farther north of Japan or over NE Japan and Hokkaido to east	6
	passing over Japan, especially over Honsyu to east	7
	Zonal shape anticyclone	8
	Passing along Pacific coast of Japan or in the Pacific	9
IV	**Frontal pattern** Front running west-cost over Japan with stational nature	10
	Front running west-east along the Pacific coast of Japan or in the Pacific with stational nature	11
V	**South-high-north-low patterns by occupation of the subtropical North Pacific middle latitude anticyclone over Japan**	12
VI	**Typhoo n pattern** Typhoon Center locates south of Kyusyu	13
	Typhoon locates in the area from Yellow sea to the Pacific through Honsyu.	14
	typhoon locates in the N Japan, mainly over Hokkaido	15

5. 2 Precipitation model each weather type (Plan)

We calculate the probability of no rain day and average precipitation amount in rain day and in each weather type. Precipitation model is used equation (7) based on exponential distribution in addition to error factor.

$$P = Ii * (ln(R)) * (1 + e) \ldots (7)$$

where *P: daily* precipitation, *Ii: average* precipitation at rain day in each weather type, *R: uniform* random variables, *e: uniform* random variables

Fig 1 shows simulation flow of this method

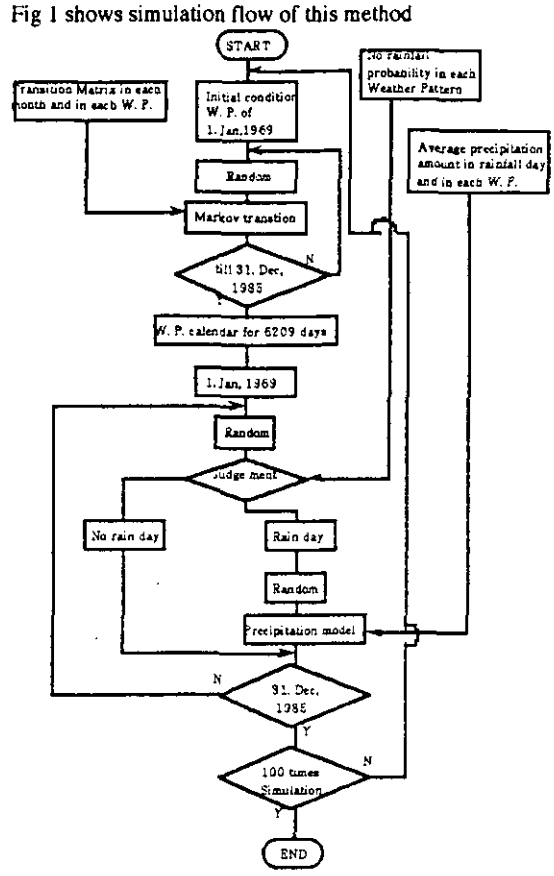

Fig 1 Flow Chart

6. Future works

We are scheduled to extract the change of transition matrix under global warming condition from MRI-GCM and to execute simulation of precipitation and runoff calculation.

References

1)McCabe, G.J & Wolock, D.M: Sensitivity of irrigation demand in a humid temperature region to hypothetical climate change. Water Resource Bulletin, Vol.28, pp535-543, 1992

2)Tokioka, T & Saito M: Numerical experiments on the characteristics of ocean/continent scale climate change in global warming produced by CO2 increase. Proceedings of the workshop on the effects of global climate change on hydrology and water resources at Catchment scale, p.57-66, 1992

3) M. Yoshino, "Kikougaku", p.213-221

4)S. Yamakawa, "Kikougaku kenkyu houkoku", No14, 1988

5)Hey, L.E, & McCabe, G.J. etc.: *Simulation of* precipitation by weather type analysis. Water resource research, Vol.27, pp.493-501, 1991

Development and Application of UNEP/GRID Global Environmental Datasets

Contact Person: Research Program Manager, Hideo Harasawa
Center for Global Environmental Research(CGER), National Institute for Environmental Studies (NIES), Environment Agency of Japan

Keywords: UNEP/GRID, global environmental data, data creation, environmental index

1. Background

The Global Resources Information Database (GRID) was established as an environmental information system of the United Nations Environment Programme (UNEP) in 1985. The CGER/NIES joined this worldwide information database network in May 1991 as the 8th cooperating center, which is called GRID-Tsukuba center. The major missions are 1) to play a leading role in interfacing with GRID users in Japan and neighbor countries, 2) to provide datasets acquired or generated in environmental research and monitoring activities of NIES and CGER, and to disseminate them to GRID users, 3) to develop GIS and remote sensing technology and to provide technical support to GRID users in these field, and 4) to promote the user of global environmental data in science and policy making[1]. In particular, regarding the second mission, development of global socio-economic datasets is considerably expected to the GRID-Tsukuba center.

2. Objective

Global datasets obtained from UNEP/GRID and other data distribution organizations are in general voluminous, so that it is the first step to extract necessary parameters in specific research areas, and then, pre-process and visualize them for further analysis of the global environment issues. The purpose of this study is to develop and apply global environmental datasets for research and decision making. The high-speed computing power and mass storage capacity of the Super-computer system (NEC SX-3) has been used for this development work. Geographic information system (GIS) which is running on the workstation system connecting to the super-computer by network has been used for overlaying and indexing of environmental data to generate original global environmental datasets. Although this development work is now going on, the outline of this study along with preliminary results is demonstrated in this report.

3. Method

3.1 Pre-processing of voluminous datasets

Table 1 shows some of typical global datasets which are needed for global environmental research such as assessing impacts of global warming on the environment and society. These data have been obtained from UNEP/GRID and other international and national data distribution organizations. For example, the size of soil data by the United Nations Food and Agriculture Organization (FAO) is about 60Mb, and the daily output of General Circulation Model (GCM) by the Geophysical Fluid Dynamics Laboratory (GFDL) in Q-flux is more than 600Mb. These large datasets are not effectively dealt with in workstations and mainframe computers in general.

3.2 Geographic Information System

UNEP/GRID has processed the global datasets produced by the various data distribution organizations into geographically referenced and gridded datasets using GIS system in workstations and personal computers. UNEP/GRID has used the GIS systems such as ARC/INFO and GRASS for workstations and IDRISI for personal computers. Using GIS, data can be more readily combined, compared and correlated with each other. In addition, the data can be converted between various scales and projections. In this study, ARC/INFO and GRASS was used for data processing and visualization.

4. Results

4.1 Global warming scenarios

Global warming scenarios are essential in assessing impacts of global warming on the environment and society. The difference in temperature between the current and possible CO_2 doubling conditions from GCM results obtained through GFDL were added to the temperature distribution in long term average produced by the International Institute for Applied System Analysis (IIASA). The GCM data has a spacial precision, 7.5 ° in longitude by 4.5 ° in latitude. On the other hand, IIASA's temperature data has 0.5 ° by 0.5 °. Figure 1 shows this combined temperature distribution. GIS system is very flexible in calculating combined effects of several parameters and displaying the result in any given region or area.

4.2 Creation of socio-economic datasets

Atlas of the environment and population in each country is very good information source for national socio-economic situations. Based on the population atlas of China, coastal lines and national, provincial, and prefectural boundaries were digitized and stored in ARC/INFO format. At the same time, prefectural population from the national statistics of population in China were recorded in the database of ARC/INFO. Figure 2 shows the base map of China population distribution. This national datasets can be of use to generate gridded population map, which will be fundamental inputs to estimate national CO_2 emission.

4.3 Vulnerability assessment of sea level rise

As an example of indexing using GIS, several global datasets were applied to assess vulnerability of coastal areas in Asian region to sea level rise. The Intergovernmental Panel on Climate Change (IPCC) working group I estimates that possible sea level rise would be 65 cm in 2100, which might cause significant impacts on low lying land in coastal region and small island nations in Pacific region. Three datasets such as elevation, gridded population, and damage of typhoon

are used to assess the vulnerability. Its severity is categorized into 4 considering the magnitude of the above three parameters. Figure 3 shows the result. More precise analysis is needed, but this map can be used as a screening tool in assessing impacts of sea level rise in coastal regions[2].

The above examples are demonstrated here as preliminary products, and not final ones. Through this work, the super-computer and its workstation system are considerably useful in dealing with large-size datasets, especially in developing global environmental database for analysis of various issues of global environment.

Acknowledgements

This study has been conducted as a part of development of global environmental database of CGER/NIES and UNEP/GRID-Tsukuba.

References

1. CGER, UNEP/GRID Tsukuba, 1991.
2. Machida, S. et al., Database System for Vulnerability Assessment to Sea Level Rise: An Asia-Pacific VA, Paper presented at the IPCC Eastern Hemisphere Workshop on the Vulnerability of Sea-level Rise and Coastal Zone Management, 1993.

Table 1 UNEP/GRID and other global datasets

Parameters	Spacial Resolution	Temporal Resolution	Size (Mb)
Political Boundary	1:1 mil.	none	80
Elevation	5'	none	18
Soils	2'	none	58
Soil degradation	1:10 mil.	none	4
GVI	16km	weekly	2.2
Precipitation	0.5°	monthly	0.2
Temperature	0.5°	monthly	0.2
Cloudiness	0.5°	monthly	0.2
Asia mosaic GVI	1km	1989	15
GCM Q-flux	4.5°* 7.5°	1*,2*CO_2	640
GCM transient	7° * 10°	monthly	300

Figure 1 Temperature distribution produced using GIS

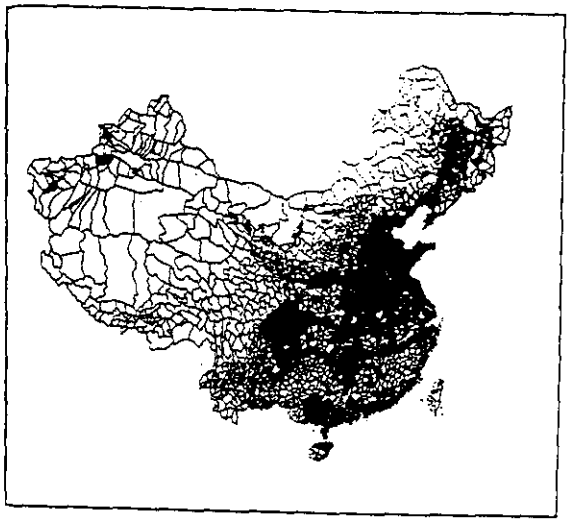

Figure 2 Population distribution in China

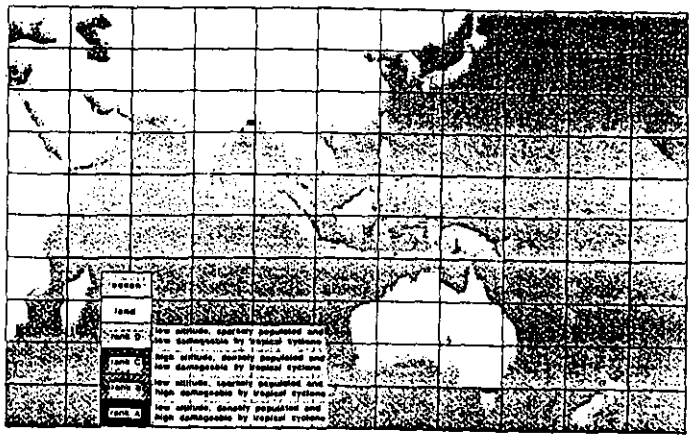

Figure 3 Overlay analysis of land eleveation, population and damage of typhoon

Neural Networks as Applied to SAR of Toxicity of Dioxins

Contact Person Dr. Hiroshi Ichikawa
Hoshi College of Pharmacy, Shinagawa, Tokyo 142

Research Organization
Special Research Projects
Theme Studies for a systematic evaluation of chemosphere under highly advanced technology
Researchers T. Fujii (Environmental Chemistry Division)
H. Ichikawa (Guest Scientist from Hoshi College of Pharmacy)
H. Shinoda (Guest Scientist from Toyama Medical and Pharmaceutical University)

Keywords dioxins, dibenzofurans, neural networks, nonlinear analysis

1. Background

Dioxins (polychlorodibenzo-*p*-dioxins: PCDDs) consist of 75 isomers with different physicochemical characteristics. Among them 2,3,7,8-tetrachloro-dibenzo-*p*-dioxin (TCDD) has been considered to be most hazardous to human as well as animals. Although toxicity, generally, is a total effect including absorbtion, metabolism, and secretion, Poland showed that the toxicity of a PCDD is measurable quantitatively by the induction potency of a specific enzyme.[1]

Aromatic hydrocarbon hydroxydase (AHH), for example, is one of metabolizing enzymes, which includes NADPH-cytochrome P-450 and exists in microsome and the outer membrane of the nucleus. The induction potency of 2,3,7,8-tetrachlorodibenzodioxin (TCDD) is $3X10^4$ times stronger than that of 3-methylcholanthrene, a typical AHH inducer. 2,3,7,8-Tetrachlorodibenzofuran (TCDF) is also a potent AHH inducer.[2] On the other hand, it is known that hexachlorodioxins and dibenzofurans exhibit low induction potencies even if they have chlorine atoms at 2, 3, 7, and 8 positions. This indicates that the induction ability is controlled by the structure, size, and other physicochemical parameters.

2. Objective

Studies on quantitative structure-activity relationship (QSAR) have been carried out especially to lead out effective drugs. The first QSAR method is the model proposed by Hansch and co-workers.[2-5] The success of this method has prompted may workers to reexamine the drivation of the Hnasch equation using the principles of theoretical pharmacology.[6,7] This model, the free energy model,[8] and its elaborations[9] have been by far most widely used.[10] This may be due to its direct conceptual linkage to established physical organic chemical principles. However, the method has been totally dependent on the multiregression analysis. This causes the problems of orthogonality of the variables as well as their linearities against the biological intensity.

Recently, the neural network has been the center of attention in the field of pattern recognition. The neural network is one of typical parallel-distributed processing methods and is a computer-based system derived from simplified concept of the brain in which a number of nodes, called processing elements or neurons, are interconnected in a netlike structure. Since the characteristics of the neural network have been found to be suitable for the data processing in which the relationship between the cause and its results cannot be exactly defined, we believe that the effective application of such neural networks may afford a new method in the analysis for the cause of toxicity.

So far, we have investigated the operation of perceptron-type neural networks in an attempt to apply them to (Q)SAR studies in developing new drugs. Useful results have been shown eslewhere.[11-18] Meanwhile, we have discovered that if the number of neurons of the output layer is set to be one with a linear operational function which is allowed to take an analog value, this type of neural network (named the MR-type neural network) operates as a generalized (nonlinear multiregression) analysis.[15] The MR-type neural network is easily applied to QSAR analysis. Because of its nonlinear operation, the results were remarkable in both fitting and prediction.

To investigate the structure-activity relationship (SAR) of PCDDs and PCDFs, we applied neural network (NN) methods. The relationships of the induction potency and the following physico-chemical parameters are investigated: (1) mother structures, i. e., dibenzo-*p*-dioxins vs dibenzofurans, (2) ionization energy, (3) heats of formation, (4) dipole moments, (4) energy levels of the lowest unoccupied MOs (LUMO), and (5) the number of chlorine atoms. Generally, the relationship between a biological activity and a physicochemical parameter is nonlinear. Thus, we applied the descriptor mapping technique to a characteristic case.

3. Method

The detailed theory of the standard operation of a neural network with the back-propagation algorithm has been shown elesewhere.[11-18] and here a brief theory is described. The number of the layer is arbitrary and generally consists of n layers. However a three-layer network is enough as shown in Fig. 1. In an MR-type neural network,[13] the number of the neuron in the output layer is set to be one, for which a linear function is used as the activation function. The data are input to the neurons of the input layer and are output from those of the output layer. The value of a neuron (O_j) at the nth layer can be expressed by,

$$O_j = \beta h(y_j) + (1-\beta) y_j = f(y_j) \quad (1)$$

$$h(y_j) = 1/[1+\exp(-\alpha y_j)] \quad (2)$$

$$y_j = (\sum_i W_{ij} x_i) - \theta_j \quad (3)$$

There, we used a combination function of the sigmoid and linear functions as the operational function (Eq. 1) for the second-layer neurons, where β is a parameter which controls the mixing degree. The training of the network is carried out until the sum of the squared errors, $\Sigma(O_j - t_j)^2$, becomes small enough based on the following equations,

$$\delta W_{ij}^{(n-1,n)} = -d_j^{(n)} x_i \varepsilon \quad (4)$$

$$d_j^{(3)} = (O_j - t_j) g'(y_j) \quad (5)$$

$$d_j^{(2)} = (\sum_l W_{jl}^{(2,3)} d_l^{(3)}) f'(y_j) \quad (6)$$

Here, $f'()$ and $g'()$ are the derivative functions of the activation functions for the second- and third-layer neurons, ε is a parameter which determines a shift for correction in back-propagation. If Eq. 1 is adopted as the operation function, the derivative function, f', in Eq. 5 or 6 is,

$$f'(y_j) = \alpha\beta h(y_j)[1-h(y_j)] + 1 - \beta \quad (7)$$

To know the degree on the contribution of the input to the output, it is necessary to obtain partial derivative of the output with respect to the input. The method of the derivation has been described in ref. 18. The partial derivatives of the output in a third-layer neuron, $O_j^{(3)}$, with respect to an input parameter, x_i, is given by,

$$\frac{\partial O_j^{(3)}}{\partial x_i} = \sum_k f'(y_k) W_{ik}^{(1,2)} g'(y_j) W_{kj}^{(2,3)} \quad (8)$$

where the superscript on W expresses the connected layers.

Table 1. Physicochemical Parameters of PCDDs and PCDFs Calculated by MNDO

	Ip	Hf	Dp	LUMO
dioxin				
1,2,3,4	9.035	-36.864	3.727	-1.349
1,2,7,8	9.118	-42.722	2.467	-1.336
1,3,7,8	9.149	-44.717	1.323	-1.358
2,3,7,8	9.148	-44.641	0.021	-1.396
1,2,3,4,7	9.230	-43.274	1.999	-1.538
1,2,3,7,8	9.278	-46.018	1.248	-1.554
1,2,4,7,8	9.275	-46.288	1.093	-1.511
1,2,3,4,7,8	9.395	-46.999	0.335	-1.711
dibenzofuran				
1,2,3,7	9.495	-7.244	1.260	-1.514
2,3,4,7	9.526	-7.070	2.660	-1.513
2,3,4,8	9.529	-7.353	2.145	-1.473
2,3,7,8	9.559	-8.892	0.414	-1.510
1,2,3,7,8	9.672	-11.248	1.594	-1.695
1,2,3,7,9	9.641	-8.089	2.196	-1.700
1,2,4,6,8	9.647	-13.080	0.292	-1.629
1,2,4,7,8	9.671	-12.367	1.255	-1.673
1,3,4,7,8	9.647	-12.331	0.956	-1.727
2,3,4,7,8	9.697	-11.176	0.979	-1.695
2,3,4,7,9	9.683	-12.141	1.832	-1.706
1,2,3,4,7,8	9.783	-13.102	0.424	-1.893
1,2,3,6,7,8	9.827	-13.461	0.688	-1.863
2,3,4,6,7,8	9.822	-13.196	2.086	-1.859

Ip: Ionization energy (eV), Hf: Heat of formation (kcal/mol), Dp: Dipole moment (debye). The data were taken from Ref. 19.

4. Resuts and Discussion

Table 1 shows physicochemical parameters calculated by the MNDO method while Table 2 shows potencies of recepter binding, AHH and EROD of PCDDs and PCDfs. The biological activity, p, is logged, multiplied by -1, and scaled between 0.1 and 0.9 before being fed as the training data. Table 3 shows averadged $\partial O/\partial x$ values, i.e., the contribution of an input parameter to the biological activity. Here, a larger absolute value indicates the strong contribution; positive and negative values indicate positive and negative contributions to the activity.

The table clearly shows that the heat of formation and dipole moment have nothing to do with the biological activity. The number of the chlorine atoms is not a much contributor either. Let us look at doxin/furan. All values are negative indicating that PCDDs are more stronger than PCDFs; This effect is substantial at the activity concerning AHH. The potential activity is found in the terms of ionization energy and LUMO. This strongly suggests that the interction between the agent and enzyme is formed by a charge-transfer interaction.

Finally, the relasionship between HOMOs and

LUMOs are analyzed by using descriptor mapping method.[18] The 3-D map in Fig. 1 indicates the nonlinear relarionship between those two parameters: They are closely related to the intensity.

Table 2. AHH/EROD induction potencies of PCDDs and PCDFs

	RB	AHH	EROD
dioxin			
2,3,7,8	$1.0X10^{-8}$	$7.2X10^{-11}$	$1.9X10^{-10}$
1,2,3,7,8	$7.9X10^{-8}$	$1.1X10^{-8}$	$1.7X10^{-8}$
1,2,7,8	$1.6X10^{-7}$	$6.1X10^{-8}$	$1.1X10^{-8}$
1,2,3,4,7,8	$2.8X10^{-7}$	$2.1X10^{-9}$	$4.1X10^{-9}$
1,3,7,8	$7.9X10^{-7}$	$5.9X10^{-7}$	$3.2X10^{-7}$
1,2,4,7,8	$1.1X10^{-6}$	$2.1X10^{-8}$	$1.1X10^{-8}$
1,2,3,4	$1.3X10^{-6}$	$3.7X10^{-6}$	$2.4X10^{-6}$
1,2,3,4,7	$6.4X10^{-6}$	$6.6X10^{-7}$	$8.2X10^{-7}$
dibonzofuran			
2,3,4,7,8	$1.5X10^{-8}$	$2.4X10^{-10}$	$1.3X10^{-10}$
2,3,4,7	$2.5X10^{-8}$	$1.8X10^{-8}$	$1.5X10^{-8}$
2,3,7,8	$4.1X10^{-8}$	$3.9X10^{-10}$	$2.0X10^{-10}$
2,3,4,6,7,8	$4.7X10^{-8}$	$6.9X10^{-10}$	$5.8X10^{-10}$
1,2,3,7,8	$7.5X10^{-7}$	$2.5X10^{-9}$	$3.1X10^{-8}$
1,2,3,7	$1.1X10^{-7}$	$2.5X10^{-5}$	$6.3X10^{-5}$
1,3,4,7,8	$2.0X10^{-7}$	$1.6X10^{-9}$	$1.4X10^{-9}$
2,3,4,7,9	$2.0X10^{-7}$	$7.9X10^{-9}$	$5.8X10^{-9}$
2,3,4,8	$2.0X10^{-7}$	$4.1X10^{-8}$	$3.8X10^{-8}$
1,2,3,4,7,8	$2.3X10^{-7}$	$3.6X10^{-10}$	$3.8X10^{-10}$
1,2,3,6,7,8	$2.7X10^{-7}$	$1.5X10^{-9}$	$1.2X10^{-9}$
1,2,3,7,9	$4.0X10^{-7}$	$8.6X10^{-8}$	$8.6X10^{-8}$
1,2,4,7,8	$1.3X10^{-6}$	$1.1X10^{-7}$	$1.5X10^{-7}$
1,2,4,6,8	$3.1X10^{-6}$	$1.0X10^{-5}$	$1.2X10^{-6}$

RB: Receptor binding. The data were taken from Ref. 2.

Table 3. Averaged $\partial 0/\partial x$ Values (Relationships between Intensity and Input Parameters)

IP	Hf	Dp	LUMO	Cl	oxin/furan
Receptor binding					
13.104	0.036	-0.330	-14.635	-4.000	-6.711
AHH					
19.924	0.062	-1.587	-11.101	-2.425	-16.783
EROD					
11.258	0.032	-1.450	-10.296	-3.629	-3.339

IP: Ionization energy, Hf: Heat of formation, Dp: Dipole moment, LUMO: Lowest unoccupied orbital, Cl: Number of chlorine atoms, oxin/furan: Preference of toxicity of mother nucleus.

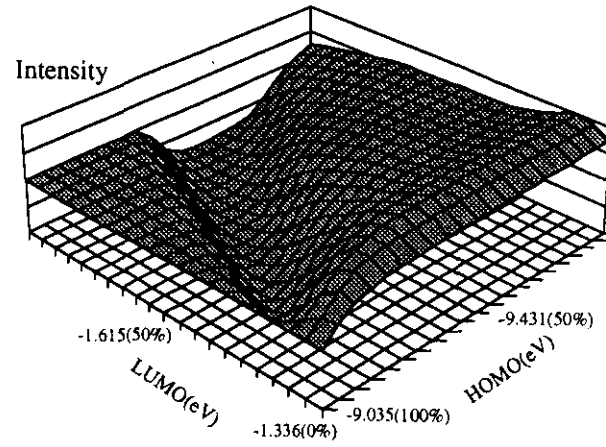

Fig.1. Descriptor mapping of HOMO and LUMO against the intensity of AHH activity.

References

1. A. Poland and A. Kende, "Origins of Human Cancer Book, B," H. Hiatt, D. J. Watson, and J. A. Winten, Eds., University of Tokyo Press, Tokyo, 1978.
2. S. H. Safe, *Ann. Rev. Pharmacol. Toxicol.*, **26**, 371 (1986).
3. C. Hansch, R. M. Muir, T. Fujita, P. Maloney, E. Geiger, and M. Streich, *J. Am. Chem. Soc.*, **85**, 2817 (1963).
4. C. Hansch and T. Fujita, *J. Am. Chem. Soc.*, **86**, 1616 (1964).
5. C. Hansch, *J. Med. Chem.*, **19**, 1 (1976).
6. V. Austel and E. Kutter, In "Drug Design," E. J. Ariens, Ed., Med. Chem. Academic Press, Vol. 10, p. 1, 1980.
7. A. Goldstein, L. Aronow, and N. S. Kalman, "Principles of Drug Action - Basis of Pharmacology," 2nd Ed.; Wiley, New York, 1974.
9. J. E. Leffler and E. Grunwald, "Rates and Equilibria of Organic Reactions," Wiley, New York, 1963.
10. For a review, see, for example, J. G. Topliss, "Quantitative Structure-Activity Relationships of Drugs," Academic Press, New York (1983).
11. T. Aoyama, Y. Suzuki, and H. Ichikawa, *Chem. Pharm. Bull.*, **37**, 2558 (1989).
12. T. Aoyama, Y. Suzuki, and H. Ichikawa, *J. Med. Chem.*, **33**, 905 (1990).
13. T. Aoyama, Y. Suzuki, and H. Ichikawa, *J. Med. Chem.*, **33**, 2583 (1990).
14. T. Aoyama and H. Ichikawa, *Chem. Pharm. Bull.*, **39**, 358 (1991).
15. T. Aoyama and H. Ichikawa, *Chem. Pharm. Bull.*, **39**, 372 (1991).
16. T. Aoyama and H. Ichikawa, *Chem. Pharm. Bull.*, **39**, 1222 (1991).
17. T. Aoyama and H. Ichikawa, *J. Chem. Inform. Comput. Sci.*, **32**, 492 (1992).
18. H. Ichikawa and T. Aoyama, *SAR and QSAR Environm. Res.*, **1**, 115 (1993).
19. C. J. Koester and R. A. Hites, *Chemosphere*, **17**, 2355 (1988).

Thermal Insulation and Condensation on Reinforced Concrete Construction

Contact Person

(Research Organization) Kazumasa WATANABE, Building Research Institute,
Ministry of Construction

Keywords: thermal insulation, condensation, reinforced concrete, heat and moisture transfer

1. Background

Corresponding to the intensified demand for energy conservation, it is normalized to add a thermal insulation on the constructions. But the insulation brings often an important condensation in it and serious damages not only to the internal finishes but also to the furnitures or to the constructions themselves and provokes healthy problems to the inhabitants because of fungus or mold that grow up under humid condition.

2. Objective

This simulation of heat and moisture simultaneous transfer has an objective to find out and distinguish the wall compositions with or without risk of condensation and their regional difference.

3. Method

The programme was developed on the basis of Matsumoto Model described with following equations.

$$\rho_w \frac{\partial \phi}{\partial t} = \frac{\partial}{\partial x}\left[D\phi \frac{\partial \phi}{\partial x} + D_T \frac{\partial T}{\partial x} \right] \quad (1)$$

$$c\rho \frac{\partial T}{\partial t} = \frac{\partial}{\partial x}\left[(\lambda + \gamma D_{Tg}) \frac{\partial T}{\partial x} + \gamma D_{\phi g} \frac{\partial \phi}{\partial x} \right] \quad (2)$$

$$\phi = F(h, T) \cong F(h) \quad (3)$$

where,

T: temperature t: time

ϕ: volumic water content x: distance

h: relative humidity ρ_w: density of liquid water

γ: evaporation heat of water c: specific heat of material

D: water diffusivity λ: thermal conductivity

ρ: density of material

subscripts: T: temperature gradient

ϕ: water content gradient

g: gas phase

The program used in this simulation was two dimentional one. It neglects the effects of following factors.
(1) Liquid water transfer; so that water transfers in the components only in the phase of vapor.
(2) Convection of air; so that it neglects the difference in direction of speed in flow of heat or moisture.
(3) Hysteresis in hygric properties; and even the sorption isotherm is linealized from the curve in the range under RH90%.
(4) Change of climate in short term; the room climate data are given as monthly average and the external climate data are given as cosine curve created on the basis of maximum and minimum daily averages in a year.
(5) Initial water content of concrete; the initial water content of each material is given as an equilibrium water content defined by the annual mean circumstances.
(6) Direct solar radiation, rain, snow and strong wind; so that the results of this calculation correspond only to the building component positioned at north side and well protected from rain and strong wind.

The properties of each material used in this simulation are shown below.

	density of dried material kg/m^3	thermal conductivity kcal/m h ℃	specific heat kcal/kg℃	vapor permeability g/m h mmHg	sorption slope wt%/rh%
fiber insulation	16	0.038	0.20	0.07	0.014
foam resin insulation	30	0.030	0.30	0.005	0.01
wood based insulation	270	0.048	0.31	0.019	0.15
sprayed resin coating	1000	0.16	0.30	0.0017	0.01
light weight mortar	1400	1.0	0.22	0.005	0.06
PVC wall paper	550	0.12	0.33	0.0015	0.01
wood fiber brd	322	0.052	0.31	0.019	0.24
polyethylen film	100	0.16	0.30	0.0000002	0.001
concrete	2300	1.3	0.19	0.0033	0.028
gypsum brd	900	0.15	0.27	0.0069	0.21

The simulation was conducted by using standardized climate data of 5 different regions: Sapporo, Akita, Sendai, Tokyo and Kagoshima, and by fixing the depth of concrete wall and by changing the specifications of finishes and insulations, especially the position of insulation to the concrete structure. The room air conditions are fixed as follow through all the regions.

	Jan	Feb	Mar	Apr	May	Jun	Jul	Aug	Sept	Oct	Nov	Dec
T℃	22.1	22.0	22.3	22.8	23.4	23.7	24.5	25.0	23.5	23.0	22.6	22.3
RH%	61.0	62.0	63.0	65.0	68.0	70.0	71.0	71.0	70.0	65.0	63.0	61.0

Result

Examples of the results of simulation are shown in the Table-1 and 2. The maximum relative humidity distribution expected in each component are figured with tone gradation representing the categories as shown below.

a) In case of concrete wall without thermal insulation:

The simulation shows that bare concrete wall produces condensation in winter in all regions but in Kagoshima. The external finishing with sprayed resin intensifies this risk of condensation whereas the internal finishing with PVC wall paper moderates this risk. The concrete wall without any finishing at both sides shows a risk of condensation both in winter and in summer.

b) The effects of different insulation systems:

The simulation shows the difference produced with different insulation systems. The fiber based insulation which has high thermal resistance but low moisture transfer resistance creates easily the condensation in the component. The foam resin insulation which has high moisture transfer resistance with higher thermal resistance shows less risk of condensation. The wood based insulation which has moisture sorptive characteristics with medium thermal and moisture transfer resistance moderates the risk of condensation.

In a large part of regions, the external insulation systems moderate well the risk of condensation. But in Kagoshima, where it is very hot and humid in summer and not so cold in winter the exeternal insulation systems cannot reduce the risk of condensation. In Kagoshima, all the thermal insulation systems calculated in this simulation show a certain risk of condensation but even the bare concrete wall without insulation shows a risk of condensation. Kagoshima seems to be a region where the thermal insulation and even the concrete construction cannot be applied. In Sapporo, only the external insulation systems can be applied.

References:

1. Vers une solution aux problemes de condensation dans la construction-Teneur en eau des materiaux poreux et condensation, Kazumasa WATANABE and Yuzo SAKAMOTO, CIB 89

2. Prevention des problemes de condensation et Historique des etudes sur le transfert simultane de chaleur et d'humidite - Formulation de base et proprietes de materiaux- , Mamoru MATSUMOTO, Japan-France Symposium on Condensation in Building, Jan 17-18, 1991

3. KENTIKU SEKKEI SIRYO SYUSEI (Collection of Design Materials for Construction), Archiectural Institute of Japan, Maruzen

4. Design Techniques of Large Scale Wood Constructions (Building Component), The Building Center of Japan

5. SHITUDO, SUIBUN KEISOKU TO KANKYO NO MONITOR (Measurement of Humidity and Moisture, Monitoring of Environment), Japan Mechanical Engineering Association, Gihodo

Maximum Relative Humidity Distribution
in Components without Thermal Insulation (Table-1)

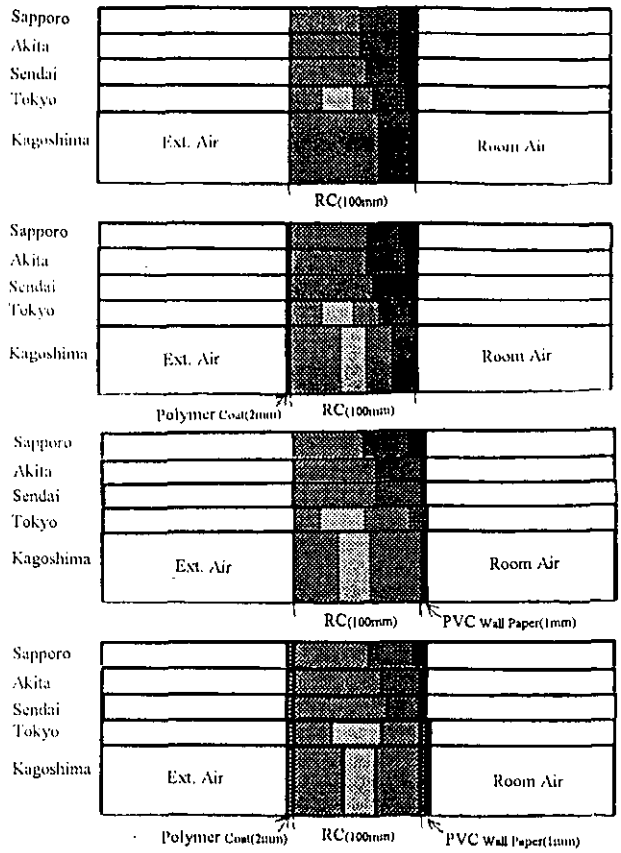

Maximum Relative Humidity Distribution
in Components with Thermal Insulation (Table-2)
--Case with Internal Application of Fiber Based Insulation--

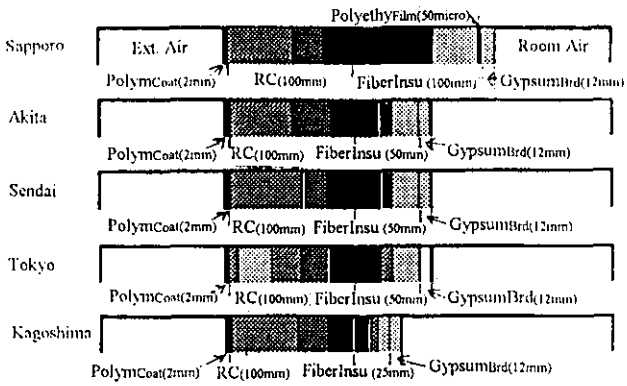

--Case with External Application of Foam Resin Insulation--